JCI The Journal of Clinical Investigation

S100A8/A9 regulates CD11b expression and neutrophil recruitment during chronic tuberculosis

Ninecia R. Scott, … , Joaquin Zuñiga, Shabaana Khader

J Clin Invest. 2020. https://doi.org/10.1172/JCI130546.

Research In-Press Preview **Immunology** **Infectious disease**

Graphical abstract

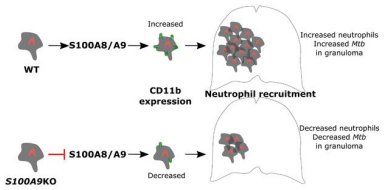

Long title: S100A8/A9 regulates CD11b expression and neutrophil recruitment during chronic tuberculosis

Ninecia R. Scott[1], Rosemary V. Swanson[1], Noor Al-Hammadi[2], Racquel Domingo-Gonzalez[1], Javier Rangel-Moreno[3], Belinda A, Kriel[4], Allison N. Bucsan[5], Shibali Das[1], Mushtaq Ahmed[1], Smriti Mehra[5], Puthayalai Treerat[1], Alfredo Cruz-Lagunas[6,7], Luis Jimenez-Alvarez[6,7], Marcela Muñoz-Torrico[6,7], Karen Bobadilla-Lozoya[6,7], Thomas Vogl[8], Gerhard Walzl[4], Nelita du Plessis[4], Deepak Kaushal[9], Thomas J. Scriba[10], Joaquín Zúñiga[6,7], and Shabaana A. Khader[1*]

[1]Department of Molecular Microbiology and Microbial Pathogenesis and [2]Division of Biostatistics, Washington University in St. Louis, St. Louis, MO; [3]Division of Allergy, Immunology and Rheumatology, Department of Medicine, University of Rochester Medical Center, Rochester, NY; [4]Division of Molecular Biology and Human Genetics, Department of Biomedical Sciences, Faculty of Medicine and Health Sciences, South African MRC Centre for Tuberculosis Research, DST and NRF Centre of Excellence for Biomedical TB Research, Stellenbosch University, Stellenbosch, South Africa; [5]Divisions of Bacteriology and Parasitology, Tulane National Primate Research Center, Covington, Louisiana, USA; [6]Laboratory of Immunobiology and Genetics, Instituto Nacional de Enfermedades Respiratorias Ismael Cosio Villegas, Mexico City, Mexico; [7]Tecnologico de Monterrey, Escuela de Medicina y Ciencias de la Salud, Mexico City, Mexico; [8]Institute of Immunology and Interdisciplinary Center for Clinical Research, University of Münster, Münster, Germany; [9]Southwest National Primate Research Center, Texas Biomedical Research Institute, San Antonio, TX; [10]South African Tuberculosis Vaccine Initiative and Institute of Infectious Disease and Molecular Medicine, Division of Immunology, Department of Pathology, University of Cape Town, Cape Town, South Africa.

*__Corresponding Author__- Shabaana A. Khader, Department of Molecular Microbiology, Campus Box 8230, 660 South Euclid Avenue, St. Louis, MO, 63110-1093, Phone: (314) 286-1590, Fax: (314) 362-1232, Email: sakhader@wustl.edu

Conflict of Interest Statement

T.J.S. is co-inventor of a patent of the 16-gene ACS signature. All other authors declare no competing financial interests.

Abstract

Neutrophil accumulation is associated with lung pathology during active tuberculosis (ATB). However, the molecular mechanism(s) by which neutrophils accumulate in the lung and contribute to TB immunopathology is not fully delineated. Using the well-established mouse model of TB, our new data provides evidence that the alarmin S100A8/A9 mediates neutrophil accumulation during progression to chronic TB. Depletion of neutrophils or *S100A8/A9* deficiency resulted in improved *Mycobacterium tuberculosis* (*Mtb*) control during chronic but not acute TB. Mechanistically, we demonstrate that following *Mtb* infection, S100A8/A9 expression is required for upregulation of the integrin molecule CD11b specifically on neutrophils, mediating their accumulation during chronic TB disease. These findings are further substantiated by increased expression of *S100A8* and *S100A9* mRNA in whole blood in human TB progressors when compared to non-progressors, and rapidly decreased S100A8/A9 protein levels in the serum upon TB treatment. Furthermore, we demonstrate that S100A8/A9 serum levels along with chemokines are useful in distinguishing between ATB and asymptomatic *Mtb*-infected latent individuals. Thus, our results support targeting S100A8/A9 pathways as host-directed therapy for TB.

Introduction

Mycobacterium tuberculosis (*Mtb*), the causative agent of the disease tuberculosis (TB), is estimated to infect one fourth of the world's population and results in ~1.6 million deaths each year (1). In addition, the emergence of multi-drug and extensively drug resistant *Mtb* strains and variable efficacy of the currently used vaccine, *Mycobacterium bovis* BCG*,* are barriers to global control of TB. Thus, more research is needed to fully understand the mechanisms of TB immunopathogenesis that can be targeted to improve host control of *Mtb* infection.

Neutrophil accumulation has been associated with TB disease in humans and mouse models of TB (2, 3). Neutrophils are the primary *Mtb*-infected cell population in the sputum, bronchoalveolar lavage (BAL), and cavities of *Mtb*-infected patients (4). In mouse models, neutrophils are amongst the first cells infected with *Mtb*, and are capable of recognizing and responding to *Mtb* infection and displaying effector functions (5, 6). Calprotectin, also known as S100A8/A9, is mainly expressed by myeloid cells, specifically neutrophils and monocytes, and is a feature of chronic inflammatory diseases such as autoimmune diseases and TB (7-9). S100A8 and S100A9 covalently form the hetero-complex protein S100A8/A9, and bind to receptors such as Toll-like receptor 4 (TLR4) and the receptor for advanced glycation end products (RAGE), which mediates a pro-inflammatory response through nuclear factor kappa-light-chain-enhancer of activated B cells (NF-κB) and nuclear factor (erythroid-derived 2)-like 2 (Nrf2) signaling (10, 11). We recently demonstrated that S100A8/A9-expressing neutrophils accumulated within TB granulomas in human and animal models of TB, and that S100A8/A9 serum levels coincided with increased neutrophil numbers and enhanced TB disease in active TB (ATB) patients (7). However, we did not fully understand the mechanism(s) by which S100A8/A9 mediates neutrophil accumulation that may promote TB disease severity.

In the current study, we demonstrate that S100A8/A9 expression mediated accumulation of lung neutrophils in chronically *Mtb*-infected mice. Additionally, the observed accumulation is mirrored

by increased *S100A8* and *S100A9* mRNA in whole blood transcriptional profiles of latently infected individuals (LTBI) who progress to ATB disease (progressors), when compared with individuals who do not progress to TB disease (non-progressors). Importantly, serum levels S100A8/A9 protein decreased rapidly upon successful TB treatment. These studies suggest that in animal models and human progressors, S100A8/A9 expression levels increase during TB progression or chronic TB disease. Consistent with a detrimental role for S100A8/A9, mice depleted of neutrophils or deficient in *S100A9* exhibit decreased *Mtb* burden in the lungs during chronic infection and TB reactivation. The improved *Mtb* control in *S100A9*KO mice coincided with reduced lung neutrophil accumulation within TB granulomas, and decreased expression of the integrin CD11b on neutrophils. Our mechanistic *in vitro* studies show that *S100A9*KO neutrophils have defective *Mtb* uptake, as well as reduced ability to upregulate CD11b integrin expression. Importantly, we demonstrate that S100A8/A9 serum levels along with chemokines are useful to distinguish between ATB patients and LTBI. Our results suggest that targeting S100A8/A9 as host directed therapy in TB would provide novel pathways that can be used as adjunct therapy to improve *Mtb* control.

Results

Depletion of neutrophils during chronic but not acute TB improves *Mtb* control

A neutrophil associated transcriptional signature was reported in ATB patients and neutrophil accumulation was associated with TB disease in mouse models (2, 3, 7). Consistent with this, neutrophils accumulated in the blood during ATB but not in asymptomatic latency in macaques infected with *Mtb* (**Figure 1A**). However, it is unclear if neutrophils play distinct roles during the acute and chronic stages of *Mtb* infection. Thus, we studied the kinetics of neutrophil accumulation in the well-established mouse model of low dose aerosol *Mtb* infection in C57BL/6J (B6) mice. Neutrophils accumulated in the lung following infection with *Mtb* HN878 early, starting

at 30 days post infection (dpi). Accumulation further increased during chronic stages of infection, starting around 60 dpi and continuing until 300 dpi (**Figure 1B**). As we observed increased neutrophil accumulation during both acute and chronic stages, we next addressed the functional role for neutrophils at the two distinct phases of *Mtb* infection. We found that treatment with 1A8 antibody, which specifically depletes neutrophils (12), during acute *Mtb* infection did not impact overall lung and spleen *Mtb* burden (**Figure 1C**). Treatment with 1A8 depleted lung neutrophils significantly, but also coincided with increased monocyte and macrophage populations and increased production of the chemokine, granulocyte-colony stimulating factor (G-CSF) (**Figure 1D and Supplemental Figure 1A)**. However, despite changes in myeloid cell accumulation, the total inflammatory area measured in the lung was not significantly altered (**Figure 1E**). In contrast, 1A8 treatment during chronic *Mtb* infection led to decreased *Mtb* burden, in both the lung and spleen (**Figure 1F).** Neutrophil depletion during chronic TB did not impact other myeloid populations (**Supplemental Figure 1B**), but there was decreased production of pro-inflammatory cytokines, such as interleukin (IL)-6 and TNF-α (**Figure 1G**). The area of lung cellular inflammation was still not impacted in mice when neutrophils were depleted during chronic infection (**Figure 1H**). These data together suggest that despite early accumulation of neutrophils, neutrophils do not significantly impact *Mtb* control during acute stages of infection. In contrast, neutrophil accumulation during chronic *Mtb* infection may have a functional role in promoting higher *Mtb* burden and contribute to increased susceptibility.

S100A8/A9 is induced during progression to TB disease in animal models and in humans. S100A8/A9 makes up 40% of the cytoplasmic protein of a neutrophil (13). In addition, we have shown that increased serum S100A8/A9 levels correlate with increased neutrophils in peripheral blood of ATB patients (7). Accordingly, we found that accumulation of S100A8/A9 levels in *Mtb*-infected mouse lungs also closely followed the accumulation of neutrophil influx in the infected lung. Early increased production of S100A8/A9 was detected between 15-30 dpi and sustained

production during chronic infection was observed after 30 dpi (**Figure 2A**). As TB disease progressed, S100A8/A9 levels increased, coinciding with the increased accumulation of neutrophils observed in chronically *Mtb*-infected lungs (**Figure 1B, and 2A**), and the S100A8/A9 levels positively correlated with the number of lung neutrophils (**Figure 2B**). Thus, we next addressed if S100A8/A9 expression also correlated with TB disease progression in humans with LTBI. Therefore, we analyzed the whole blood transcriptional mRNA levels of *S100A8* and *S100A9* in participants enrolled in the Adolescent Cohort Study (ACS) of TB progressors and matched *Mtb*-infected controls (14). Transcript levels of both *S100A8* and *S100A9* mRNA significantly increased in the TB progressors about six months prior to TB diagnosis compared to expression levels in matched healthy controls (**Figure 2C**). Our results show that both in mice and in humans, an increase in S100A8/A9 expression coincides with TB disease progression.

Thus, we next determined if serum levels of S100A8/A9 protein declined upon successful treatment in ATB patients receiving standard first line TB treatment. In ATB patients that were successfully treated, and were either cured (n = 34; **Figure 2D**) or cured but then relapsed in the following 2 years after treatment (n = 10; **Figure 2E**), the S100A8/A9 levels decreased rapidly by 2 weeks post treatment, and continued to decrease throughout treatment. However, in patients that failed TB treatment (n = 10; **Figure 2F**), the S100A8/A9 levels did not decrease significantly within the first two weeks after treatment. Together, our data show that S100A8/A9 increases during TB disease progression and levels decline sharply upon successful TB treatment.

_S100A9_ deficiency improves _Mtb_ control during chronic infection by limiting neutrophil accumulation

Our new data here shows that S100A8/A9 levels increase during chronic *Mtb* infection in mice and human TB progressors, and depletion of neutrophils during chronic infection in mice improves *Mtb* control (**Figure 1 and 2**). Therefore, we next assessed the long-term outcome of *Mtb* infection in B6 and *S100A9*KO mice (15) (which lack functional S100A8/A9) during chronic stages of

infection with *Mtb* HN878. While lung and spleen *Mtb* HN878 CFU was comparable at 50 dpi, we found that during chronic infection from 100 dpi until 300 dpi, *Mtb* CFU in the lungs of *S100A9*KO mice were significantly lower, when compared to B6 HN878-infected mice (**Figure 3, A and B**). This improved *Mtb* control was also observed during infection with another clinical strain, HN563, but not when the lab-adapted *Mtb* strain H37Rv was used (**Supplemental Figure 2, A and B)**. S100A8/A9 plays a key role in neutrophil recruitment and accumulation (16-18) and thus the absence of S100A8/A9 may promote improved *Mtb* control by altering cellular accumulation to the lung and regulating inflammation. Coinciding with the timing of improved *Mtb* control in the lungs of *S100A9*KO mice at 100 dpi, we found that neutrophil accumulation was reduced, while other myeloid subsets such as alveolar macrophages (AMs), recruited macrophages (RMs), monocytes and dendritic cells (DCs) were not significantly different in lungs of *S100A9*KO mice, when compared with B6 infected mice (**Figure 3, C and D**). However, at the later stage of chronic disease, AMs, DCs, monocytes, and neutrophils were all reduced in *S100A9*KO mice when compared with B6 infected lungs (**Figure 3, C and D**). The localization of MPO-expressing neutrophils within TB granulomas during chronic infection was also decreased in *S100A9*KO mice, suggesting that S100A8/A9 expression promoted the accumulation of neutrophils in the lung, specifically localization within TB granulomas (**Figure 3E**). Presence and maintenance of B cell follicles within lung granulomas has been associated with effective *Mtb* control through optimal macrophage activation (19). Consistent with improved protection in the lungs of *S100A9*KO infected mice at chronic stages, lung B cell follicle area was significantly enhanced within TB granulomas (**Figure 3F**). However, despite altered accumulation of neutrophils within granulomas in *S100A9*KO mice, overall inflammatory area or the specific type of inflammation (myeloid or lymphocytic) in the lungs of *S100A9*KO *Mtb*-infected mice was not significantly different when compared with *Mtb*-infected B6 mice (**Supplemental Figure 3, A and B**).

S100A8/A9 binds to RAGE (20), and delivery of RAGE inhibitor (FPS-ZM1) to *Mtb*-infected mice during the chronic stages of infection significantly decreased *Mtb* burden similar to levels

observed in *S100A9*KO mice (**Figure 4A**). Although inflammation was not significantly decreased in RAGE-treated mice, B cell follicle size was significantly increased within TB granulomas (**Figure 4, B and C**). Delivery of the RAGE inhibitor to *Mtb*-infected *S100A9*KO mice (4.89 ± 0.095 $\log_{10}$CFU) did not significantly decrease *Mtb* burden when compared to DMSO-treated *S100A9*KO *Mtb*-infected mice (5.28 ± 0.44 $\log_{10}$CFU), suggesting that the off-target effects of use of RAGE inhibitor are minimal (p-value = 0.1213). These results together suggest that absence of S100A8/A9 expression or inhibition of its receptor function both improve *Mtb* control during chronic TB. To further experimentally test the role of S100A8/A9 in TB reactivation and disease progression, we used the Cornell mouse model of TB reactivation where mice were infected with *Mtb*, treated with antibiotics, following which reactivation of *Mtb* was assessed. Our data show that while B6 mice that received antibiotic chemotherapy reactivated significantly elevated *Mtb* CFU in the lung, *S100A9*KO mice exhibited significantly lower rates of reactivation and harbored overall lower lung *Mtb* CFU when compared with B6 mice, with 8 of 14 mice exhibiting no detectable lung *Mtb* CFU (**Figure 4D**). In conjunction with lower *Mtb* CFU, while inflammation was not altered, neutrophil accumulation was significantly decreased in lung granulomas of *S100A9*KO mice **(Figure 4, E and F**). These results suggest that while S100A8/A9 expression coincides with neutrophil accumulation and improved *Mtb* control, S100A8/A9 expression did not directly regulate inflammation during TB.

S100A8/A9 expression regulates CD11b expression on neutrophils during chronic TB

As neutrophil accumulation was significantly decreased in *S100A9*KO *Mtb*-infected mice, we next determined whether surface expression of the integrin CD11b, a key molecule in leukocyte adhesion and migration (21), was differentially expressed in myeloid cells in *S100A9*KO *Mtb*-infected mice when compared with B6 *Mtb*-infected mice. We observed that CD11b surface expression was significantly decreased within lung neutrophils in *S100A9*KO *Mtb*-infected mice during chronic stages of infection, whereas lung monocytes and RMs had no significant changes

in CD11b expression (**Figure 5A**). Similar decrease in CD11b expression on lung neutrophils was observed when *S100A9*KO mice were infected with *M.bovis* BCG by the pulmonary route (**Supplemental Figure 4**). Gr-1 (Ly6G/Ly6C) surface expression was also assessed, but no significant changes were seen in aforementioned other lung myeloid cell populations during both acute and chronic stages of infection in *S100A9*KO mice when compared with B6 *Mtb*-infected mice (data not shown). As myeloid cells such as neutrophils and monocytes are among the primary producers of S100A8/A9 (9, 22), we addressed if adoptive transfer of $CD11b^+$ cells producing S100A8/A9 can reverse the improved *Mtb* control seen in *S100A9*KO *Mtb*-infected mice. Accordingly, $CD11b^+$ cells transferred into *S100A9*KO mice resulted in increased lung *Mtb* burden, suggesting that a CD11b myeloid population was contributing to the increased susceptibility during *Mtb* infection (**Figure 5B**). This was not because of transfer of *Mtb* within $CD11b^+$ transferred cells, as colocalization of *Mtb* with S100A9 expression was minimal in transferred cells (**Supplemental Figure 5**). These data were corroborated by decreased lung protein levels of neutrophil attracting chemokines CXCL-1 and CXCL-2 in *S100A9*KO mice during chronic infection (**Figure 5C**). Taken together, absence of S100A8/A9 during chronic *Mtb* infection reduces neutrophil localization, decreased expression of CD11b expression on neutrophils, and adoptive transfer of CD11b cells reversed the protection observed in *S100A9*KO *Mtb*-infected lung.

S100A8/A9 regulates CD11b expression on neutrophils during *Mtb* infection

Our data points to a critical role for S100A8/A9 in regulating CD11b expression specifically on neutrophils to modulate accumulation into the lung. To mechanistically address the role of S100A8/A9 in regulation of CD11b expression on neutrophils and *Mtb* control, bone marrow derived neutrophils were infected with reporter expressing *Mtb,* and *Mtb* infection and neutrophil marker expression was assessed. While B6 neutrophils were more readily infected with *Mtb, S100A9*KO neutrophils showed significantly decreased infected neutrophils (**Figure 6A**). Consistent with our data from lung neutrophils, CD11b expression was significantly upregulated

on B6 *Mtb*^{hi} neutrophils but not as highly induced in *S100A9*KO *Mtb*^{hi} neutrophils (**Figure 6B**). *S100A9*KO neutrophils expressed lower levels of CD11b even in uninfected controls, as published before (15), suggesting that while S100A8/A9 regulates the expression of CD11b at homeostatic levels, this effect is much more profound upon *Mtb* infection. However, in B6 neutrophils, the fold induction of CD11b upon Mtb infection was 1.96, compared with 2.42 in *S100A9*KO mice. Similar results were obtained when Gr-1 and CD18 levels were measured on *S100A9*KO *Mtb*-infected neutrophils, when compared with B6 *Mtb*-infected neutrophils (**Figure 6B**). This coincided with increased induction of mRNA for signaling receptors such as *TLR2*, *TLR4*, and phagocytic receptors such as *C-type lectin receptor, Macrophage inducible* Ca^{2+}*-dependent lectin receptor* (*MINCLE*) which play a role in phagocytosis of Mtb (23); (24) but not *formyl peptide receptor 1* (*FPR1*) or *DECTIN-1* (**Figure 6C**). This increased expression of phagocytic receptors on *S100A9*KO neutrophils also coincided with increased production of proinflammatory cytokines such as IL-6 and TNF-α in *Mtb*-infected neutrophil supernatants, when compared with B6 *Mtb*-infected neutrophils (**Figure 6D**). We also assessed whether *Mtb*-infected *S100A9*KO neutrophils were deficient in chemotactic ability when compared with *Mtb*-infected B6 neutrophils, and found that the ability of *S100A9*KO neutrophils to migrate toward supernatants from *Mtb*-infected epithelial cells was not impaired (**Figure 6E**). To address if live *Mtb* infection was required for CD11b upregulation, we then tested if stimulation with heat killed (HK) *Mtb*, or components of *Mtb* will similarly regulate the S100A8/A9-dependent effects on CD11b regulation. We found that HK *Mtb* and stimulation with culture filtrate protein (CFP) and cell wall components (CW) of *Mtb* similarly induced an S100A9-dependent CD11b upregulation on neutrophils, suggesting that live *Mtb* infection was not necessary (**Figure 6F**). Since S100A8/A9 is known to induce NF-κB signaling, we also wanted to understand the role of NF-κB signaling in mediating CD11b upregulation. We isolated neutrophils from IKK$^{fl/fl}$ LysM^{Cre} mice, which lack canonical IKK and NF-κB signaling in LysM-expressing cells. We found that lack of NF-κB signaling reduced *Mtb* infection in neutrophils **(Figure 6G),** and NF-κB signaling was required for upregulation of

CD11b and Gr-1 on *Mtb*-infected neutrophils (**Figure 6G**). These results together demonstrate that absence of S100A8/A9 expression on neutrophils significantly impacts *Mtb* uptake and CD11b induction following *Mtb* infection, in part dependent on NF-κB signaling.

S100A8/A9 along with chemokines can distinguish between ATB and LTBI

Our data demonstrate that *S100A8/A9* mRNA levels increased during progression to TB in humans and rapidly decrease upon successful TB treatment. Thus, we wanted to next address if serum S100A8/A9 levels can be used to distinguish ATB patients from healthy LTBI and uninfected healthy controls (HC). S100A8/A9 serum protein levels were significantly higher in ATB patients compared to HCs (**Table 1, Figure 7A**). We also found increased S100A8/A9 serum levels in LTBI Tuberculin Skin Test (TST^+) and Quantiferon+ (QFT^+) house hold contacts of ATB patients, and LTBI TST^+ QFT^+ individuals with occupational exposure to TB, when compared with uninfected HCs (**Figure 7A**). These results suggest that S100A8/A9 levels could serve as an easily measurable surrogate of TB disease progression in LTBI individuals. Additionally, we assessed if increased S100A8/A9 serum protein was only increased during ATB or was also increased in other acute and chronic inflammatory pulmonary diseases. While S100A8/A9 serum protein levels were not higher in patients with Chronic Obstructive Pulmonary Disease (COPD), S100A8/A9 serum levels were much higher in influenza infected patients when compared with levels in ATB patients (**Figure 7A, Table 1**). These results suggest that S100A8/A9 serum measurements may distinguish between ATB and LTBI, while taking into consideration clinical symptoms which may confound the measurements.

As CXCL-1 and CXCL-10 serum levels were additionally increased in ATB patients (**Table 1**), we next sought to understand whether combining S100A8/A9 with CXCL-1 and CXCL-10 serum protein levels will improve biomarker performance for distinguishing ATB from LTBI and HC than S100A8/A9 alone (7). Median serum biomarker concentrations, with interquartile ranges, across the three groups of participants are included in **Table 2**. The medians were the lowest in the uninfected HCs for all biomarkers, followed by levels in LTBI, and the highest expression was

noted in the ATB group. When influenza and ATB groups were compared, expression of both CXCL-1 and S100A8/A9 was higher in influenza infected patients, when compared with levels in ATB patients (**Table 2**). Overall and pairwise comparisons were listed in Table 3, where the differences in the distribution of the biomarkers across all levels were significant when comparisons were made between ATB and LTBI, as well as ATB and HC. For a threshold of 114 pg/ml, CXCL-1 could differentiate between ATB and HC groups with a sensitivity of 88.4% (95% CI, 0.78-0.96) and a specificity of 61.5% (95% CI, 0.42-0.80); while for CXCL-10, a threshold of 302 pg/ml would differentiate between ATB and HC with a sensitivity of 86.5% (95%CI, 0.76-0.94) and a specificity of 57.7% (95% CI, 0.38-0.76). For S100A8/A9, a threshold of 1805 pg/ml would differentiate between ATB and HC with a sensitivity of 92.3% (95% Cl, 0.84-0.98) and a specificity of 76.9% (95% Cl, 0.57-0.92). Notably, S100A8/A9 levels were the only significant determination when LTBI and HCs were compared pairwise and not when CXCL-1 and CXCL-10 were determined for pairwise comparisons between the LTBI vs HC (**Table 2**). Furthermore, receiver operating characteristic (ROC) analysis was applied to appraise the diagnostic values of the 3 biomarkers individually and their combination (**Table 3 and 4**). Combining S100A8/A9 along with CXCL-1 and CXCL-10 into a biomarker signature improved differentiation between ATB and HCs (0.9467, 95% Cl, 0.88-1.0) when compared with utilizing CXCL-10 and S100A8/A9 as combined biomarker signatures (0.9268, 95% Cl, 0.85-0.99, **Table 3 and 4. Figure 7B**).

Discussion

Neutrophils have recently been implicated as drivers of immunopathogenesis of TB in human and animal models (2, 7, 25). However, the molecular mechanisms by which neutrophils regulate TB immunopathogenesis are not clearly understood. In this study, we demonstrate that neutrophils accumulate during progression to TB disease in *Mtb*-infected humans and mice, and play a detrimental role during chronic TB disease in mice. Additionally, S100A8/A9 levels mirror neutrophil accumulation in the lungs of mice, and *S100A9* deficiency in mice results in improved

Mtb control during chronic disease. We show that the mechanism by which S100A8/A9 contributes to increased TB disease pathogenesis is by regulating the expression of the integrin CD11b, which is required for neutrophil accumulation in the lung (15, 17). Furthermore, *S100A9* deficiency also reduces TB reactivation in mice, and use of RAGE inhibition results in improved *Mtb* control. Finally, our human studies suggest that S100A8/A9 levels along with expression of chemokines such as CXCL-1 and CXCL-10 may serve to distinguish between LTBI and ATB from HCs. Together, our results demonstrate that S100A8/A9 play pivotal functions in regulating neutrophil accumulation during TB, primarily through their effects on CD11b expression, thus providing novel insights into the immunopathogenesis of TB.

Although neutrophil accumulation has been associated with increased disease in mouse and NHP models, as well as human TB, it is still unclear whether neutrophils have protective or pathological functions in *Mtb* infection (2, 26-29). Despite neutrophils being one of the first cell types infected with *Mtb* (5), our results show that neutrophil depletion during acute *Mtb* infection in the B6 resistant strain has no significant impact on *Mtb* control or TB pathology. Indeed, in highly susceptible mouse strains such as I/St inbred mice, neutrophil depletion during acute stages may similarly improve *Mtb* control and pathology (30). Our data show that depletion of neutrophils during chronic *Mtb* infection improves *Mtb* control, and clearly establishes a detrimental role for neutrophils during the chronic stages of *Mtb* infection. Additionally, that the levels of lung S100A8/A9 correlate with neutrophil accumulation during chronic TB in mice, suggests a threshold of neutrophil accumulation may likely be required for the detrimental effects of neutrophils and S100A8/A9 proteins during TB. Additionally, during very late stages of infection, it is possible that the threshold is no longer needed, as other compensatory effects may mediate immunopathogenesis. During chronic inflammation, S100A8/A9 proteins are important in the generation and recruitment of myeloid-derived suppressor cell (MDSC) (31). Accumulation of mycobacterial permissive and immunosuppressive polymorphonuclear- and mononuclear MDSCs have also been reported in chronic *Mtb* infection in both mice and humans (32),(33).

These immunoregulatory cells localize to the peri-necrotic regions of chronic granulomas in the lungs of murine- and non-human primate TB models, signifying host failure of *Mtb* replication control (34), (33), (35). Although the presence of $CD11b^{low}Gr\text{-}1^{hi}$ $Ly6G^{hi}Ly6C^{lo}$ PMN-MDSC were not specifically investigated here, it is possible that the MDSCs are included in the $CD11b^{+}Gr\text{-}1^{+}$ gate used in the current study. Interestingly, while both neutrophil depletion and S100A8/A9 deficiency improved *Mtb* control, overall inflammatory lung disease was not impacted. In the case of neutrophil deficiency, it is possible that transient depletion of neutrophils was not sufficient to impact overall inflammation and prolonged neutrophil depletion may be required to impact lung pathology. During S100A8/A9 deficiency, while overall inflammatory disease was trending towards decreased inflammation, these data were not significant. However, the reduced accumulation of neutrophils into TB granulomas coincided with increased formation of B cell containing granulomas, which our studies in mice and NHPs have previously shown to be associated with improved *Mtb* control through enhanced macrophage activation (19, 36, 37). Furthermore, increased expression of *S100A8* and *S100A9* mRNA in LTBI who progress to pulmonary TB is likely due to inflammatory events associated with progression of disease. These data along with the overall reduced TB reactivation seen in *S100A9*KO in the Cornell mouse model implicates S100A8/A9 expression in mediating TB disease progression. Together, our results demonstrate that neutrophils and S100A8/A9 may play key roles in modulating TB immunopathogenesis by driving neutrophil accumulation.

A mechanism by which S100A8/A9 regulates TB pathogenesis is likely by directly regulating CD11b expression on neutrophils. While *S100A9* deficiency did not impact CD11b expression on neutrophils during the early stages of *Mtb* infection, deficient mice express lower CD11b levels on neutrophils during chronic TB and BCG infection. In contrast, in *S100A9*KO bone marrow neutrophils, CD11b expression is significantly lower in uninfected controls, and upon *Mtb* infection, upregulate CD11b to a lesser extent than B6 bone marrow neutrophils. Considering the baseline differences in CD11b expression in bone marrow neutrophils, it is intriguing why

differences in CD11b expression do not occur in *S100A9*KO mice until day 100 following *Mtb* infection. The nature of the microenvironment (e.g. presence of other pro-inflammatory chemokines, prolonged *Mtb* infection and stimulation, etc.) may contribute to differences observed in *in vitro* studies and *ex vivo* isolated neutrophils. Additionally, it is of considerable interest that while *S100A9*KO mice are protected from infection with a clinical *Mtb* isolate, HN878, *S100A9*KO mice do not show any protection when infected with a lab-adapted *Mtb* strain, H37Rv. Thus, our data suggest that S100A8/A9 may play homeostatic roles in regulating CD11b expression in bone marrow neutrophils, which following infection and likely induction of inflammatory signals, these effects may be amplified. Our data showing that *S100A9*KO neutrophils upon *Mtb* infection induce higher levels of phagocytic receptor expression including *TLR2*, *TLR4* and *MINCLE*, and coincident increased expression of IL-6 and TNF-α suggest that one mechanism by which *S100A9*KO mice exhibit better *Mtb* control *in vivo* during chronic TB could be due to increased *Mtb* uptake and role for neutrophil in *Mtb* clearance. Neutrophil chemotaxis has been associated with cytoskeletal reorganization and actin polymerization and regulation. *S100A9* deficient neutrophils had actin defects when responding to IL-8 stimulation, suggesting that S100A9 has a role in cytoskeletal dynamics and reorganization (15). Despite our studies showing that *S100A9*KO neutrophils do not exhibit any defects in chemotactic migration towards *Mtb*-infected epithelial cell supernatants, it is possible that functional actin coordinates cell surface integrin regulation (e.g. CD11b/CD18), could impact neutrophil migration and adhesion *in vivo* and will be tested in future studies. Together, this suggests that S100A8/A9 expression in the lung may induce chemokines that mediate neutrophil accumulation, potentially directly act as a chemoattractant for neutrophils (17), but also by upregulating the expression of CD11b to amplify neutrophil migration into the lung. In addition, upon recruitment to the lung, *Mtb* infection induced S100A8/A9 proteins may regulate phagocytic receptor expression on neutrophils enabling increased *Mtb* infection of neutrophils. Together, these S100A8/A9-dependent mechanisms increase *Mtb* susceptibility and likely mediate immunopathology.

S100A8/A9 is known to interact with TLR4 and RAGE, while CD11b expression can be driven by interactions with TLR4 on neutrophils (38, 39). Thus, S100A8/A9 may engage TLR4 and RAGE to upregulate CD11b expression on neutrophils. Adoptive transfer of $CD11b^+$ cells increased susceptibility in *S100A9*KO mice, suggesting that $CD11b^+$ immune populations, namely neutrophils or monocytes expressing S100A8/A9, are the likely cellular population mediating increased susceptibility during chronic TB. The utilization of RAGE inhibitor, FPS-ZM1, is protective in animal models of emphysema and Alzheimer's disease (11, 40). During chronic TB, we show that transient use of RAGE inhibitors is protective and is sufficient to decrease lung *Mtb* burden, but not lung inflammation. Additionally, our data that RAGE inhibitors does not further improve *Mtb* control in *S100A9*KO chronically *Mtb*-infected mice suggest that the effect is S100A8/A9 dependent rather than through the interaction of RAGE with its other ligands such as advanced glycation end products (AGE) and high-mobility group protein (B) 1 (HMGB1). Whether use of RAGE inhibitor limits neutrophil accumulation and thus reduces the *Mtb* niche is not fully explored and should be the focus of future studies. Excitingly, our data showing that S100A8/A9 deficiency delays TB reactivation suggests that RAGE inhibitors may be potentially used as host directed therapeutics in combination with current antibiotic regimens to improve *Mtb* control and should be further studied.

The rapid diagnostic test for detection of TB recommended by the World Health Organization (WHO) is an automated PCR assay that detects mycobacteria in sputum expectorated by patients. However, access remains restricted in low resource settings, and sputum-based microscopy to identify *Mtb* still remains the most commonly used diagnostic for TB, but this method is primarily capable of identifying ATB patients. Therefore, new non-sputum based screening tools for identifying individuals with ATB are required so that they can be prioritized for clinical investigation and treatment. Blood biomarkers that can differentiate progression of LTB to subclinical disease and ATB, failure of TB treatment and TB relapse would provide additional tools to improve TB diagnosis and combat the global TB epidemic. Several studies have explored

the use of host transcriptional biosignatures as diagnostic biomarkers for progression of TB and to predict risk of human TB disease (2, 41). Although these studies propose the use of transcriptional gene signatures as screening or triage tests for TB, the costs and technology associated with RT-PCR or RNA sequencing may still limit use of these biomarkers as diagnostic in low resource setting. Our published studies have shown that ATB patients in India, Mexico and South Africa all reliably exhibit increased expression of serum S100A8/A9 proteins when compared with HC (7), and now in QFT^{+}LTB individuals. Serum is more amenable to developing a simple screening test that may be easier to translate into a point of care format (e.g. the Quantum Blue assay, which works for serum and faeces). Additionally, our new studies also show that S100A8/A9 along with chemokine such as CXCL-1 and CXCL-10 serum protein levels reliably able to differentiate between ATB and HC, and although less effective but still significantly can discriminate between ATB and QFT^{+} LTB individuals. Furthermore, that S100A8/A9 is not significantly increased during other chronic pulmonary diseases such as COPD cohort suggests that S100A8/A9 may be useful as a biomarker for a triage test to rule out individuals who do not have TB, such that biomarker+ individuals then get followed up for further TB diagnosis. One limitation of the use of S100A8/A9 and chemokines is that acute respiratory infections such as influenza also result in high expression of S100A8/A9 and CXCL-1. Detailing the expression of these biomarkers in other acute bacterial infections will be useful criteria for future studies. Interestingly, S100A8/A9 could also show initial potential as an early indicator for successful TB treatment, as S100A8/A9 levels decreased significantly 2 weeks post treatment initiation in cured TB patients, and did not decrease in TB patients which failed treatment. Thus, further validation of the use of S100A8/A9, CXCL-1, and CXCL-10 in different geographical cohorts and in treatment failure and relapse studies will be useful and timely.

In summary, our studies have mechanistically described a pivotal role for S100A8/A9 proteins in mediating TB pathogenesis through regulation of CD11b and neutrophil recruitment. Additionally, our experimental studies targeting the S100A8/A9 signaling pathway project a novel pathway for

host directed therapeutics for TB. A more mechanistic understanding of the role of S100A8/A9 proteins further validates the development of S100A8/A9 and related biomarkers as novel diagnostics for TB.

Methods

Mice and NHP *Mtb* infection

C57BL/6 (B6) mice were purchased from Jackson Laboratory (Bar Harbor, ME). *S100A9*KO was obtained from Dr. Thomas Vogl (15) and mice were bred within the Washington University in St. Louis animal facility. Both sexes between the ages of 6-8 weeks were used. All mice were maintained and used in accordance with the approved Institutional Animal Care and Use Committee (IACUC) guidelines at Washington University in St. Louis. *Mtb* strains were cultured and mice were aerosol infected with ~100 colony forming units (CFU), as described previously (19). At specific time points post infection, lungs were harvested, homogenized, and serial dilutions of tissue homogenates plated on 7H11 agar plates to determine *Mtb* CFU. For reactivation experiments, mice were treated with rifabutin (Sigma) (100 mg/L) and isoniazid (Sigma) (200 mg/L) for 6 weeks and mouse tissue was then harvested at 140 dpi. For rhesus macaques infected with *Mtb*, we used clinical data stored in the Animal Records System (ARS) at the Tulane National Primate Research Center. Macaques were chosen if they were experimentally infected with *Mtb* (either CDC1551, Erdman or H37Rv strains) during 2007-2015 and exhibited either ATB or were latently infected. Post-infection, data were obtained weekly from animals until euthanasia or necropsy. Neutrophil percentages in the blood were obtained from complete blood counts performed at the same time as serum chemistry.

Adoptive transfer of $CD11b^+$ cells

Lung cell suspensions were prepared from the lungs of B6 mice 100 dpi following HN878 infection. $CD11b^+$ cells were enriched from the lung suspension using magnetic selection with CD11b

466 microbeads (Miltenyi Biotec, Auburn, CA) per manufacturer's instructions. 50 µl ($1x10^6$ cells) of
467 this suspension (72.4% purity) was administered intratracheally to HN878-infected mice at 100
468 dpi. These mice were harvested on 120 dpi as indicated.

469 **RAGE-inhibitor treatment**

470 RAGE signaling was inhibited starting 205 or 245 dpi as previously described (11) through daily
471 intraperitoneal (i.p.) injection of 1 mg/kg RAGE-specific blocker FPS-ZM1 (Tocris) or 0.1% (v/v)
472 DMSO in PBS (control). Mice were euthanized 15 days after treatment.

473 **Neutrophil Depletion**

474 Neutrophils were depleted as described (42) using 300 µg anti-mouse Ly6G (BioXcell) or isotype
475 IgG (Sigma). Briefly, in acute infections (less than 21 dpi), mice were given 300 µg of anti-mouse
476 Ly6G every other day between 10-20 dpi intraperitoneally (i.p). In chronic infections, mice were
477 given 300 µg of anti-mouse Ly6G every other day between 95-105 dpi via intraperitoneal (i.p.)
478 injections.

479 **Lung Cell Preparation and Flow Cytometry**

480 Lung cell suspensions were prepared, stained, collected and analyzed for flow cytometry as
481 described before (19). Fluorochrome-labeled antibodies specific for CD11b (M1/70, BD), CD11c
482 (HL3, BD), Gr-1 (RB6-8C5, eBioscience) were used in this study. Cells were collected using a
483 FACSJazz with FACS Sortware software. Cell populations were gated based on their forward by
484 side scatter characteristics and the frequency of specific cell types was analyzed using FlowJo
485 version 7.6.5 (Tree Star Inc, CA). Lung alveolar macrophages were gated as $CD11c^+$ $CD11b^-$,
486 lung myeloid dendritic cells were gated on $CD11c^+$ $CD11b^+$, neutrophils as $CD11b^+$ $Gr\text{-}1^{hi}$,
487 recruited macrophages were annotated as $CD11b^+$ $Gr\text{-}1^{lo}$, and monocytes were gated on $CD11b^+$
488 $Gr1^{int}$ cells as in Dunlap *et al* 2018 (43).

489 ***In vitro* neutrophil infections**

490 Neutrophils were isolated from the bone marrow using the mouse neutrophil isolation kit (Miltenyi
491 Biotec, Auburn, CA). Neutrophils were infected at an MOI of 1 for three hours. Neutrophil uptake

was derived from neutrophil infection with *Mtb* HN878-mCherry. CD11b MFI was also assessed in neutrophils treated with heat-killed *Mtb* HN878 ($1x10^6$ CFU) or *Mtb* HN878 culture filtrate protein and cell wall extracts (10 µg/ml). Fluorochrome-labeled antibodies specific for CD11b (M1/70, BD), CD18 (M18/2, Biolegend), Gr-1 (RB6-8C5, eBiosciences), were used in this study.

***In vitro* neutrophil chemotaxis assay**

Neutrophils were isolated from the bone marrow of B6 or *S100A9*KO using the mouse neutrophil isolation kit (Miltenyi Biotec, Auburn, CA). Neutrophils were infected at an MOI of 1 for one hour, and then transferred to the upper compartments of a transwell plate separated by a 5-µm polycarbonate membrane (Corning). Supernatants from *Mtb*-infected epithelial cells (Supe.), or HBSS supplemented with 1% FCS (gravity control, Grav.) was added to the lower chambers, and the cells incubated for one hour at 37℃. Chemotaxis was assessed by flow cytometry by determining the number of neutrophils found in the lower chamber after incubation. Fluorochrome-labeled antibodies specific for CD11b (M1/70, BD), Gr-1 (RB6-8C5, eBiosciences), were used in this study.

RNA Extraction and Quantitative RT-PCR.

Total RNA was isolated from neutrophils using an RNeasy Mini kit (Qiagen, Valencia, CA, USA). cDNA was synthesized using ABI reverse transcription reagents (ABI, ThermoFisher) on a BioRad DNA Engine Thermal Cycler (BioRad, Hercules, CA, USA). Gene expression was assessed using primers from IDT (Coralville, IA, USA) and ABI, and run on a Viia7 Real-Time PCR system (Life Technologies, ThermoFisher). Expression of genes of interest (*FPR1*, *TLR2*, *TLR4*, *DECTIN* (*Clec7a*) and *MINCLE* (*Clec4e*), was normalized to *GAPDH* expression, and $\log_{10}$ fold induction over the control group was assessed using the ΔΔCT calculation.

Lung histology

Lungs from *Mtb*-infected mice were perfused with 10% neutral buffered formalin and were paraffin embedded. Lung sections were stained with hematoxylin and eosin (H&E) and processed for light

517 microscopy. Images were obtained using Zeiss Axioplan 2 microscope and were recorded with a
518 Zeiss AxioCam digital camera. Sections were probed with rabbit anti-MPO (PB9057, BosterBio;
519 dilution 1:100) and biotinylated rat anti-mouse Ly6G (clone IA8, Biolegend; dilution 1:100) to
520 detect neutrophils or with anti-B220 (clone RA3-6B2, BD Pharmingen; dilution: 1/100) to detect
521 B cells. Primary antibodies were detected with Cy3 donkey anti-rabbit IgG (711-166-152, Jackson
522 ImmunoResearch Laboratories; dilution 1:200) and Alexa Fluor 488 streptavidin (A21208,
523 Thermo Fisher Scientific; dilution 1:200). B cell follicles were assessed through the automated
524 tool of the Zeiss Axioplan 2 microscope (Zeiss, Thornwood, NY, USA), and total area and
525 average size was calculated in squared microns. Myeloid and lymphocyte areas were acquired
526 with stained slide images using a Hamamatsu Nanozoomer 2.0 HT system with NDP scan
527 image acquisition software and was quantified using Visiomorph image processing software
528 (Visiopharm, Broomfield, CO).
529 In order to calculate the percentage of inflammation per lobe, all clusters of inflammatory cells in
530 an individual lobe were systematically outlined with the automated tool of the Zeiss Axioplan
531 microscope. The total area covered by inflammation was calculated by adding all the Individual
532 areas occupied by clusters of inflammatory cells located in the interstitial, peri-bronchial and
533 perivascular regions. Next, a picture of the whole lobe was obtained with the stich tool of the Zeiss
534 axioplan microscope. Lung parenchyma, excluding empty spaces (Alveoli, bronchi and blood
535 vessel lumens), was outlined with the automated tool of the Zeiss Axioplan microscope to
536 determine the area of the lobe. Finally, the percentage of the area covered by inflammation per
537 lobe was calculated by dividing the total area covered by inflammatory cells by the total area
538 occupied by lung tissue, multiplied by 100.

539

540 **RNA sequencing data from Adolescent Cohort Study progressors and controls**

We compared gene-level mRNA expression levels of *S100A8* and *S100A9* in *Mtb*-infected adolescents enrolled into the Adolescent Cohort Study (ACS) who remained healthy during 2 years of study follow-up (controls) (n=106) or who progressed to microbiologically confirmed, active TB (progressors) (n=44), as described (14, 41). Adolescents who were Mtb^+ at enrollment, or developed ATB disease more than 6 months after *Mtb* infection was first detected were included in our analyses. Each progressor had two healthy matched controls based on age, gender, ethnicity, school of attendance, and presence or absence of prior episodes of TB disease. Participants were excluded if they were ATB^+ within 6 months of enrollment or QFT and/or TST conversion, or if they were HIV infected. Participants with diagnosed or suspected TB disease were referred to a study-independent public health physician for treatment according to national TB control programs of the country involved. RNA was extracted from PAX gene tubes and RNA-sequencing performed as described (14, 41). Prospective RNA-Seq data of progressors were realigned to the time point at which active TB was diagnosed. Differences in gene-level mRNA expression between each progressor sample and the average of demographically matched control samples were computed using the published ACS metadata (14, 41). Time To Diagnosis values were assigned to each sample according to the original definitions. The $\log_2$ fold change values between progressor and control biomarkers were modeled as a nonlinear function of Time To Diagnosis for the entire population using the smooth-spline function in R with three degrees of freedom. Ninety-nine percent confidence intervals for the temporal trends were computed by performing 2000 iterations of spline fitting after bootstrap resampling from the full dataset.

ATB cohort

We recruited patients (n = 52) with confirmed ATB. The diagnosis of ATB was made by the conventional microscopic detection of acid-alcohol resistant bacteria as well as culture of *Mtb* in Lowenstein-Jensen medium in serial, non-concentrated sputum samples, radiological studies, physical examination and clinical history. All patients with ATB were residents of the urban and

metropolitan areas of Mexico City and some patients were residents from different states of the south and central area of Mexico including Veracruz, Oaxaca, Puebla and Chiapas. Patients with ATB, excluding patients with HIV and cancer, were recruited at the INER Tuberculosis Clinic in a period between 2015 and 2017.

At the same time, household contacts of ATB patients who are $TST^{+}QFT^{+}$ LTBI (n = 36) were recruited in the first two months of diagnosis. The criteria for inclusion of contacts of ATB patients were: 1) Subjects of legal age (18 to 54) willing to sign the letter of consent; 2) Subjects in close contact with the index case of ATB and 3) Subjects willing to provide the blood samples needed to participate in the study. In addition, a group of individuals (n = 28) belonging to health personnel (resident physicians of the pulmonology specialty) and administrative medical staff of the INER, considered as an occupational risk population of which both $TST^{+}QFT^{+}$ (n=19) and $TST^{+}QFT^{-}$ (n=9) were included. Also, a group of uninfected healthy individuals ($TST^{-}QFT^{-}$) were also recruited (n=26). Only patients with ATB, LTBI, and healthy controls who agreed to participate in the study and who signed an informed consent letter were included. The study was reviewed and approved by the Institutional Research Committee with protocol number B04-15. After the consent signature, 20 ml of blood anticoagulated with EDTA and 10 ml of blood without anticoagulant was used to isolate serum for the purpose of performing the experimental analysis.

TB treatment cohort

Study participants, 34 cured and 10 relapse TB patients, and 10 patients who failed TB treatment, were enrolled and treated from TB clinics surrounding Tygerberg Hospital in Cape Town, South Africa, as a sub-study to the Pulmonary TB cohort study (April 2010 and April 2013) and the Action TB study (May 1999 and July 2002) (44, 45). Serum samples were used for the quantification of circulating S100A8/A9 concentrations. Pulmonary TB patients were all untreated at the time of enrollment with a first episode of TB. All TB patients received directly observed treatment, which

consisted of an intensive phase (2 months) of rifampicin (RIF), isoniazid (INH), pyrazinamide, and ethambutol followed by a continuation phase (4 months) of RIF and INH. Patients were aged between 20 and 65 years and clinical information on age, sex, weight, and height (BMI) was recorded. Mycobacterial culture was performed using the automated BACTEC 12B liquid radiometric method. Individuals who had two consecutive negative culture results at the end of treatment were regarded as successfully cured. Bacteriological relapse following anti-TB treatment was determined within 24 months after treatment completion. Standardized restriction fragment length polymorphism (RFLP) banding patterns generated by southern hybridization with the insertion sequence (IS) 6110 probe17 were determined in patients with recurrent TB. Episodes were classified as relapse when the strain pattern was the same. TB treatment failure was defined by a positive sputum culture at month 6 post initiation of standard treatment of drug-sensitive TB. All individuals adhered to treatment (>80% of drugs taken) and were infected with drug sensitive *Mtb* strains. No distinct differences in strain types were observed between failed and cured patients. Patients were excluded if they previously had TB; MDR TB, were HIV positive, presented with diabetes, malignancy, lung cancer, chronic bronchitis, or sarcoidosis, were on steroid treatment or were pregnant. Chest X-rays (CXRs) were only obtained at baseline and were read independently in a blinded fashion by a pulmonologist or clinician.

G-CSF, IL-6, TNF-α, CXCL-2, S100A8/A9, CXCL-1 and CXCL-10 protein quantification

Levels of G-CSF, IL-6 and TNF-α, CXCL-1 and CXCL-2 in mouse lung homogenates were measured using a mouse Luminex assay (Linco/Millipore). Circulating levels of S100A8/A9 were measured in serum samples by ELISA using the DuoSet ELISA Development kit for human S100A8/S100A9 heterodimer (Cat: DY8226, R&D Systems Inc., Minneapolis, MN, USA), according to the manufacturer's instructions. Serum samples were diluted 1:4000 in reagent diluent (1% BSA in PBS). Absorbance was read at 450 nm and 540 nm (for wavelength correction) using the Synergy HT microplate ELISA reader (BioTek Inc., Winooski, VT, USA). Serum levels

of CXCL-1 were measured by CXCL-1 Quantikine ELISA Kit (Cat: DGR00B, R&D Systems Inc.) according to the manufacturer's instructions. For this assay, samples were diluted 1:2. Absorbance was read at 450nm and 540nm using the Synergy HT microplate ELISA reader (BioTek Inc.). Serum levels of CXCL-10 were assessed by Luminex using the Bio-Plex Pro CXCL10 Set (Bio-Rad Laboratories, Inc., Hercules, CA, USA) according to the manufacturer's instructions. The samples were read in a BioPlex-200 instrument. The results were analyzed using the BioPlex software V 4.1 (Bio-Rad Laboratories).

Statistics

Differences between the means of two groups were analyzed using the two tailed Student's t-test in GraphPad Prism 5 or Graphpad Prism 8 (La Jolla, CA). Multiple groups were analyzed using 1-way ANOVA with Tukey's or Dunnett's post-test analysis, or Mixed Effects Analysis of 1-way ANOVA with Dunnett's post-test as indicated. Differences are noted as significant when a **p-value** is less than or equal to 0.05 (*), less than or equal to 0.01 (**), less than or equal to 0.001 (***), and less than 0.0001 (****).

The distribution of the biomarkers in human samples was examined and expressed as a median and interquartile range (IQR). The differences in the distributions across the groups was evaluated using the Kruskal-Wallis nonparametric test where the Dwass, Steel, Critchlow-Fligner Method was used to check for Pairwise Two-Sided Multiple Comparison Analysis (46-48). The diagnostic efficiency of the individual biomarkers and their combinations was assessed by ROC analysis where the AUC and associated 95% confidence intervals (CIs) were determined. A nonparametric approach was used to compare the correlated ROC curves without adjustments for pairwise comparisons (49). Logistic regression analysis was performed to determine the predictive probability of these biomarkers on the each of the outcome combinations. The level of significance was set to 0.05 and all analysis were 2-sided. Statistical analyses and figures were performed with SAS 9.4 (SAS Institute Inc., Cary, NC, USA).

Study Approval

For human studies, written informed consent from participants, and parents/legal guardians where applicable was received under a protocols approved by the Ethics Committee of the Instituto Nacional de Enfermedades Respiratorias (Mexico City) and the Human Research Ethics Committee of the Faculty of Health Sciences (Cape Town) and the City of Cape Town City Health. Protocols involving the use of animals were approved by IACUC at Washington University in St. Louis and Tulane National Primate Research Center. All of the experiments were performed in accordance with the protocols.

Authors Contributions

Conceptualization: SAK, Mouse experiments: NRS, RVS, RDG, JRM, SD, MA, PT; NHP experiments: ANB, SM; Human analysis: NRS, NA, BAK, ACL, LJA, MMT, KBL, GW, NdP; writing of the original draft of the manuscript: NRS, NA, RDG, and SAK; review and editing of the manuscript: NRS, RVS, NA, JRM, SD, TV, NdP, DK, TJS, JZ and SAK; funding acquisition: DK, TJS, JZ, and SAK; study supervision: SAK.

Acknowledgements

This work was supported by Washington University in St. Louis, NIH grant HL105427 to S.A.K., AI123780 to S.A.K., T.S., and D.K., AI111914 to S.A.K. and D.K., NIH/NHLBI T32 HL007317-40 to NS, and NIH Shared Instrumentation Grant S10 RR0227552. This work was supported by Grants from the Interdisciplinary Center of Clinical Research of the University of Muenster (Vo2/014/09) and the German Research Foundation (DFG) CRC 1009 B8 to T.V. This work was supported by the National Council of Science and Technology of Mexico (Consejo Nacional de Tecnología de México, CONACYT, Grant FONSEC SSA/IMSS/ISSSTE/S0008-2017-1/290512. We thank, Drs. Shyamala Thirunavukkarasu and Nicole Howard, and Ms. Lan Lu and Ms. Misty Veschak (Washington University in St. Louis) for technical support.

664

Tables

Table 1: Descriptive Statistics (Median and Interquartile Range) of biomarkers in Active TB, Latent TB, Healthy controls, and Influenza infected patients.

	Active TB		Latent TB		Healthy C		Influenza	
	Median	IQR[A]	Median	IQR[A]	Median	IQR[A]	Median	IQR
CXCL1	145.92	122.23, 184.57	129.66	100.1, 158.01	106.84	98.12, 134.61	364.52	219.78, 508.03
CXCL10	1140.84	469.07, 2231.9	254.94	173.72, 344.72	257.4	126.53, 414.44	1306.98	475.25, 2456.59
S100A8/A9	5990.69	2906.09, 10050.35	1595.7	1075.03, 2821.5	960.37	490.84, 1771.91	11254.61	9266.72, 12263.68

[A]Interquartile Range (IQR)

Table 2: Differences in the distribution across the three individual biomarkers

	P-value[A]	P value for Pairwise comparisons[B]			
		Active TB vs Latent TB	Active TB vs Healthy C	Latent TB vs Healthy C	Active TB vs Influenza[A]
CXCL1	0.0001	0.0198	<.0001	0.1539	<.0001
CXCL10	<.0001	<.0001	<.0001	0.997	0.5789
S100A8/A9	<.0001	<.0001	<.0001	0.0206	0.0006

[A]Kruskal Wallis Test

[B]Dwass, Steel, Critchlow-Fligner Method

Table 3: Area Under the Curve (AUC) of the Model Biomarker Combinations

Models	AUC	LL 95% CI	UL 95% CI
Active TB vs Health Controls			
S100A8/A9	0.9083	0.8373	0.9793
CXCL1	0.8003	0.6930	0.9076
CXCL10	0.8536	0.7685	0.9386
S100A8/A9+CXCL1+CXCL10[A]	**0.9467**	**0.8893**	**1.0000**
CXCL10+ S100A8/A9[A]	**0.9268**	**0.8633**	**0.9903**
CXCL10+CXCL1	0.9157	0.8448	0.9866
CXCL1+ S100A8/A9[A]	**0.9231**	**0.8537**	**0.9925**
Active TB vs Latent TB			
S100A8/A9	0.8575	0.7897	0.9254
CXCL1	0.6421	0.5454	0.7387
CXCL10	0.8665	0.797	0.9359
S100A8/A9+CXCL1+CXCL10[A]	**0.8968**	**0.8398**	**0.9538**
CXCL10+ S100A8/A9[A]	**0.8925**	**0.8326**	**0.9524**
CXCL10+CXCL1[A]	**0.8841**	**0.8201**	**0.9480**
CXCL1+ S100A8/A9	0.8581	0.7905	0.9256
Latent TB vs Health Controls			
S100A8/A9[A]	**0.6777**	**0.5434**	**0.8120**
CXCL1	0.6230	0.5082	0.7378
CXCL10	0.5049	0.3610	0.6488
S100A8/A9+CXCL1+CXCL10[A]	**0.6701**	**0.5507**	**0.7895**
CXCL10+S100A8/A9[A]	**0.6593**	**0.5227**	**0.7958**
CXCL10+CXCL1	0.6148	0.4994	0.7303

[A]Bolded are the top 3 model combinations in terms of the AUC

Table 4: Comparison of the models top 3 AUCs within each group using the ROC macro (reference: http://support.sas.com/kb/25/addl/fusion_25017_6_roc.sas.txt)

Models	p-value for pairwise and overall c statistic comparisons
Active TB vs Health Controls	
S100A8/A9+CXCL1+CXCL10 vs CXCL10+S100A8/A9[A]	**0.0451**
S100A8/A9+CXCL1+CXCL10 vs CXCL10+CXCL1	0.1857
CXCL10+CXCL1 vs S100A8/A9+CXCL10	0.5331
Overall p-value	0.1040
Active TB vs Latent TB	
S100A8/A9+CXCL1+CXCL10 vs CXCL1+ S100A8/A9	0.3419
S100A8/A9+CXCL1+CXCL10 vs CXCL10+ S100A8/A9	0.3937
S100A8/A9+CXCL1 vs S100A8/A9+CXCL10	0.7048
Overall p-value	0.3937
Latent TB vs Health Controls	
S100A8/A9+CXCL1+CXCL10 vs CXCL10+ S100A8/A9	0.8355
S100A8/A9+CXCL1+CXCL10 vs S100A8/A9	0.8824
S100A8/A9+CXCL10 vs S100A8/A9	0.1628
Overall p-value	0.3768

[A]significant comparisons are in bold

References

1. Organization WH. Geneva: World Health Organization; 2018.
2. Berry MPR, Graham CM, McNab FW, Xu Z, Bloch SAA, Oni T, et al. An interferon-inducible neutrophil-driven blood transcriptional signature in human tuberculosis. *Nature.* 2010;466(7309):973-7.
3. Dorhoi A, Desel C, Yeremeev V, Pradl L, Brinkmann V, Mollenkopf HJ, et al. The adaptor molecule CARD9 is essential for tuberculosis control. *J Exp Med.* 2010;207(4):777-92.
4. Eum SY, Kong JH, Hong MS, Lee YJ, Kim JH, Hwang SH, et al. Neutrophils are the predominant infected phagocytic cells in the airways of patients with active pulmonary TB. *Chest.* 2010;137(1):122-8.
5. Blomgran R, and Ernst JD. Lung neutrophils facilitate activation of naive antigen-specific CD4+ T cells during Mycobacterium tuberculosis infection. *J Immunol.* 2011;186(12):7110-9.
6. Ernst JD. The immunological life cycle of tuberculosis. *Nat Rev Immunol.* 2012;12(8):581-91.
7. Gopal R, Monin L, Torres D, Slight S, Mehra S, McKenna KC, et al. S100A8/A9 proteins mediate neutrophilic inflammation and lung pathology during tuberculosis. *Am J Respir Crit Care Med.* 2013;188(9):1137-46.
8. Rammes A, Roth J, Goebeler M, Klempt M, Hartmann M, and Sorg C. Myeloid-related protein (MRP) 8 and MRP14, calcium-binding proteins of the S100 family, are secreted by activated monocytes via a novel, tubulin-dependent pathway. *J Biol Chem.* 1997;272(14):9496-502.
9. Voganatsi A, Panyutich A, Miyasaki KT, and Murthy RK. Mechanism of extracellular release of human neutrophil calprotectin complex. *J Leukoc Biol.* 2001;70(1):130-4.
10. Goyette J, and Geczy CL. Inflammation-associated S100 proteins: new mechanisms that regulate function. *Amino Acids.* 2011;41(4):821-42.
11. Lee H, Park JR, Kim WJ, Sundar IK, Rahman I, Park SM, et al. Blockade of RAGE ameliorates elastase-induced emphysema development and progression via RAGE-DAMP signaling. *Faseb j.* 2017;31(5):2076-89.
12. Daley JM, Thomay AA, Connolly MD, Reichner JS, and Albina JE. Use of Ly6G-specific monoclonal antibody to deplete neutrophils in mice. *Journal of leukocyte biology.* 2008;83(1):64-70.
13. Edgeworth J, Gorman M, Bennett R, Freemont P, and Hogg N. Identification of p8,14 as a highly abundant heterodimeric calcium binding protein complex of myeloid cells. *The Journal of biological chemistry.* 1991;266(12):7706-13.
14. Scriba TJ, Penn-Nicholson A, Shankar S, Hraha T, Thompson EG, Sterling D, et al. Sequential inflammatory processes define human progression from M. tuberculosis infection to tuberculosis disease. *PLoS Pathog.* 2017;13(11):e1006687.
15. Manitz MP, Horst B, Seeliger S, Strey A, Skryabin BV, Gunzer M, et al. Loss of S100A9 (MRP14) results in reduced interleukin-8-induced CD11b surface expression, a polarized microfilament system, and diminished responsiveness to chemoattractants in vitro. *Mol Cell Biol.* 2003;23(3):1034-43.
16. Raquil MA, Anceriz N, Rouleau P, and Tessier PA. Blockade of antimicrobial proteins S100A8 and S100A9 inhibits phagocyte migration to the alveoli in streptococcal pneumonia. *J Immunol.* 2008;180(5):3366-74.
17. Ryckman C, Vandal K, Rouleau P, Talbot M, and Tessier PA. Proinflammatory activities of S100: proteins S100A8, S100A9, and S100A8/A9 induce neutrophil chemotaxis and adhesion. *J Immunol.* 2003;170(6):3233-42.

18. Vandal K, Rouleau P, Boivin A, Ryckman C, Talbot M, and Tessier PA. Blockade of S100A8 and S100A9 suppresses neutrophil migration in response to lipopolysaccharide. *J Immunol.* 2003;171(5):2602-9.
19. Slight SR, Rangel-Moreno J, Gopal R, Lin Y, Fallert Junecko BA, Mehra S, et al. CXCR5(+) T helper cells mediate protective immunity against tuberculosis. *J Clin Invest.* 2013;123(2):712-26.
20. Ehlermann P, Eggers K, Bierhaus A, Most P, Weichenhan D, Greten J, et al. Increased proinflammatory endothelial response to S100A8/A9 after preactivation through advanced glycation end products. *Cardiovasc Diabetol.* 2006;5:6.
21. Ding ZM, Babensee JE, Simon SI, Lu H, Perrard JL, Bullard DC, et al. Relative contribution of LFA-1 and Mac-1 to neutrophil adhesion and migration. *J Immunol.* 1999;163(9):5029-38.
22. Pechkovsky DV, Zalutskaya OM, Ivanov GI, and Misuno NI. Calprotectin (MRP8/14 protein complex) release during mycobacterial infection in vitro and in vivo. *FEMS Immunol Med Microbiol.* 2000;29(1):27-33.
23. Lee W-B, Kang J-S, Yan J-J, Lee MS, Jeon B-Y, Cho S-N, et al. Neutrophils Promote Mycobacterial Trehalose Dimycolate-Induced Lung Inflammation via the Mincle Pathway. *PLOS Pathogens.* 2012;8(4):e1002614.
24. Gopalakrishnan A, Dietzold J, Verma S, Bhagavathula M, and Salgame P. Toll-like Receptor 2 Prevents Neutrophil-Driven Immunopathology during Infection with Mycobacterium tuberculosis by Curtailing CXCL5 Production. *Infect Immun.* 2019;87(3):e00760-18.
25. Keller C, Hoffmann R, Lang R, Brandau S, Hermann C, and Ehlers S. Genetically determined susceptibility to tuberculosis in mice causally involves accelerated and enhanced recruitment of granulocytes. *Infect Immun.* 2006;74(7):4295-309.
26. Eruslanov EB, Lyadova IV, Kondratieva TK, Majorov KB, Scheglov IV, Orlova MO, et al. Neutrophil responses to Mycobacterium tuberculosis infection in genetically susceptible and resistant mice. *Infect Immun.* 2005;73(3):1744-53.
27. Kisich KO, Higgins M, Diamond G, and Heifets L. Tumor necrosis factor alpha stimulates killing of Mycobacterium tuberculosis by human neutrophils. *Infection and immunity.* 2002;70(8):4591-9.
28. Lombard R, Doz E, Carreras F, Epardaud M, Le Vern Y, Buzoni-Gatel D, et al. IL-17RA in Non-Hematopoietic Cells Controls CXCL-1 and 5 Critical to Recruit Neutrophils to the Lung of Mycobacteria-Infected Mice during the Adaptive Immune Response. *PloS one.* 2016;11(2):e0149455.
29. Tan BH, Meinken C, Bastian M, Bruns H, Legaspi A, Ochoa MT, et al. Macrophages acquire neutrophil granules for antimicrobial activity against intracellular pathogens. *Journal of immunology (Baltimore, Md : 1950).* 2006;177(3):1864-71.
30. Yeremeev V, Linge I, Kondratieva T, and Apt A. Neutrophils exacerbate tuberculosis infection in genetically susceptible mice. *Tuberculosis (Edinburgh, Scotland).* 2015;95(4):447-51.
31. Sinha P, Okoro C, Foell D, Freeze HH, Ostrand-Rosenberg S, and Srikrishna G. Proinflammatory S100 Proteins Regulate the Accumulation of Myeloid-Derived Suppressor Cells. *The Journal of Immunology.* 2008;181:4666-75.
32. du Plessis N, Loebenberg L, Kriel M, von Groote-Bidlingmaier F, Ribechini E, Loxton AG, et al. Increased Frequency of Myeloid-derived Suppressor Cells during Active Tuberculosis and after Recent Mycobacterium tuberculosis Infection Suppresses T-Cell Function. *American Journal of Respiratory and Critical Care Medicine.* 2013;188(6):724-32.
33. Knaul JK, Jörg S, Oberbeck-Mueller D, Heinemann E, Scheuermann L, Brinkmann V, et al. Lung-Residing Myeloid-derived Suppressors Display Dual Functionality in Murine

Pulmonary Tuberculosis. *American Journal of Respiratory and Critical Care Medicine.* 2014;190(9):1053-66.
34. Obregón-Henao A, Henao-Tamayo M, Orme IM, and Ordway DJ. Gr1(int)CD11b+ myeloid-derived suppressor cells in Mycobacterium tuberculosis infection. *PLoS One.* 2013;8(11):e80669-e.
35. Domingo-Gonzalez R, Das S, Griffiths KL, Ahmed M, Bambouskova M, Gopal R, et al. Interleukin-17 limits hypoxia-inducible factor 1α and development of hypoxic granulomas during tuberculosis. *JCI Insight.* 2017;2(19):e92973.
36. Kaushal D, Foreman TW, Gautam US, Alvarez X, Adekambi T, Rangel-Moreno J, et al. Mucosal vaccination with attenuated Mycobacterium tuberculosis induces strong central memory responses and protects against tuberculosis. *Nature communications.* 2015;6:8533.
37. Foreman TW, Mehra S, LoBato DN, Malek A, Alvarez X, Golden NA, et al. CD4+ T-cell-independent mechanisms suppress reactivation of latent tuberculosis in a macaque model of HIV coinfection. *Proceedings of the National Academy of Sciences of the United States of America.* 2016;113(38):E5636-44.
38. Pruenster M, Kurz AR, Chung KJ, Cao-Ehlker X, Bieber S, Nussbaum CF, et al. Extracellular MRP8/14 is a regulator of beta2 integrin-dependent neutrophil slow rolling and adhesion. *Nature communications.* 2015;6:6915.
39. Vogl T, Tenbrock K, Ludwig S, Leukert N, Ehrhardt C, van Zoelen MA, et al. Mrp8 and Mrp14 are endogenous activators of Toll-like receptor 4, promoting lethal, endotoxin-induced shock. *Nat Med.* 2007;13(9):1042-9.
40. Hong Y, Shen C, Yin Q, Sun M, Ma Y, and Liu X. Effects of RAGE-Specific Inhibitor FPS-ZM1 on Amyloid-beta Metabolism and AGEs-Induced Inflammation and Oxidative Stress in Rat Hippocampus. *Neurochem Res.* 2016;41(5):1192-9.
41. Zak DE, Penn-Nicholson A, Scriba TJ, Thompson E, Suliman S, Amon LM, et al. A blood RNA signature for tuberculosis disease risk: a prospective cohort study. *Lancet.* 2016;387(10035):2312-22.
42. Kang DD, Lin Y, Moreno JR, Randall TD, and Khader SA. Profiling early lung immune responses in the mouse model of tuberculosis. *PLoS One.* 2011;6(1):e16161.
43. Dunlap MD, Howard N, Das S, Scott N, Ahmed M, Prince O, et al. A novel role for C-C motif chemokine receptor 2 during infection with hypervirulent Mycobacterium tuberculosis. *Mucosal Immunol.* 2018;11(6):1727-42.
44. Hesseling AC, Marais BJ, Kirchner HL, Mandalakas AM, Brittle W, Victor TC, et al. Mycobacterial genotype is associated with disease phenotype in children. *The International Journal of Tuberculosis and Lung Disease.* 2010;14(10):1252-8.
45. Ronacher K, Chegou NN, Kleynhans L, Djoba Siawaya JF, du Plessis N, Loxton AG, et al. Distinct serum biosignatures are associated with different tuberculosis treatment outcomes. *Tuberculosis (Edinburgh, Scotland).* 2019;118:101859.
46. Douglas CE, and Michael FA. On distribution-free multiple comparisons in the one-way analysis of variance. *Communications in Statistics - Theory and Methods.* 1991;20(1):127-39.
47. Olkin I. *Contributions to probability and statistics; essays in honor of Harold Hotelling.* Stanford, Calif.: Stanford University Press; 1960.
48. Steel RGD. A Rank Sum Test for Comparing All Pairs of Treatments. *Technometrics.* 1960;2(2):197-207.
49. Zhou. Xiao-Hua, Obuchowski. Nancy A., and K. MD. *Statistical Methods in Diagnostic Medicine.* New Jersey: John Wiley & Sons; 2011.

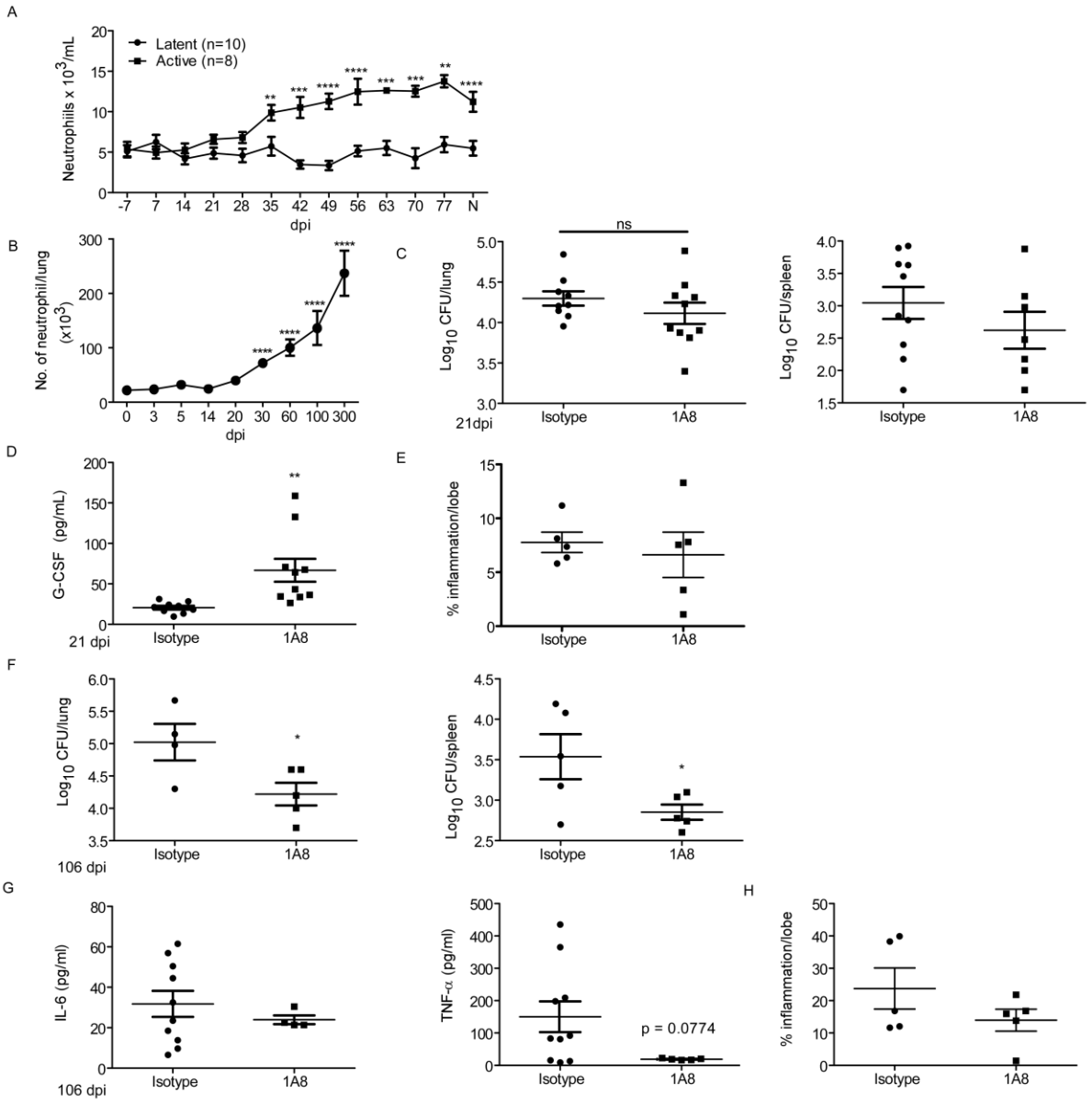

Figure 1. Neutrophil depletion during chronic TB improves *Mtb* control. (A) The number of blood neutrophils from Rhesus macaques with ATB (n=8) or LTBI (n=10) were measured at dpi following *Mtb* infection or at necropsy (N). B6 mice (n = 5-13) were aerosol-infected with ~100 CFU Mtb HN878. (B) Neutrophil accumulation was determined by flow cytometry at dpi. B6 mice were infected with *Mtb* HN878 and administered IgG (n = 5-10) or 1A8 (n = 5-10, 300 µg/dose) i.p. every other day. (C) Bacterial burden in the lung and spleen was determined by plating on 21 dpi. (D) Lung homogenates were analyzed for G-CSF protein expression by ELISA on 21 dpi. (E) Pulmonary inflammation was quantified on formalin-fixed paraffin embedded (FFPE) lung sections from 21 dpi samples stained with H&E. B6 mice were infected with HN878 and administered IgG (n = 4-5) or 1A8 (n = 4-5, 300 µg/dose) i.p. every other day. (F) Bacterial burden in the lung and spleen was determined by plating on 106 dpi. (G) Lung homogenates were analyzed to measure levels of IL-6 and TNF-α proteins at 106 dpi using Luminex assays. (H) Pulmonary inflammation was quantified on FFPE lung sections from 106 dpi tissues stained with H&E. Figures are depicting 1 experiment representative of 2, or combined data from multiple experiments. The data points represent the mean (±SEM) of values. (A) 2-way ANOVA, (B) Student's t-test between 0 and indicated dpi, (C-G) Student's t-test between isotype and 1A8 treated mice. P = 0.05 (*), P = 0.01 (**), P = 0.001 (***), and P = 0.0001 (****).

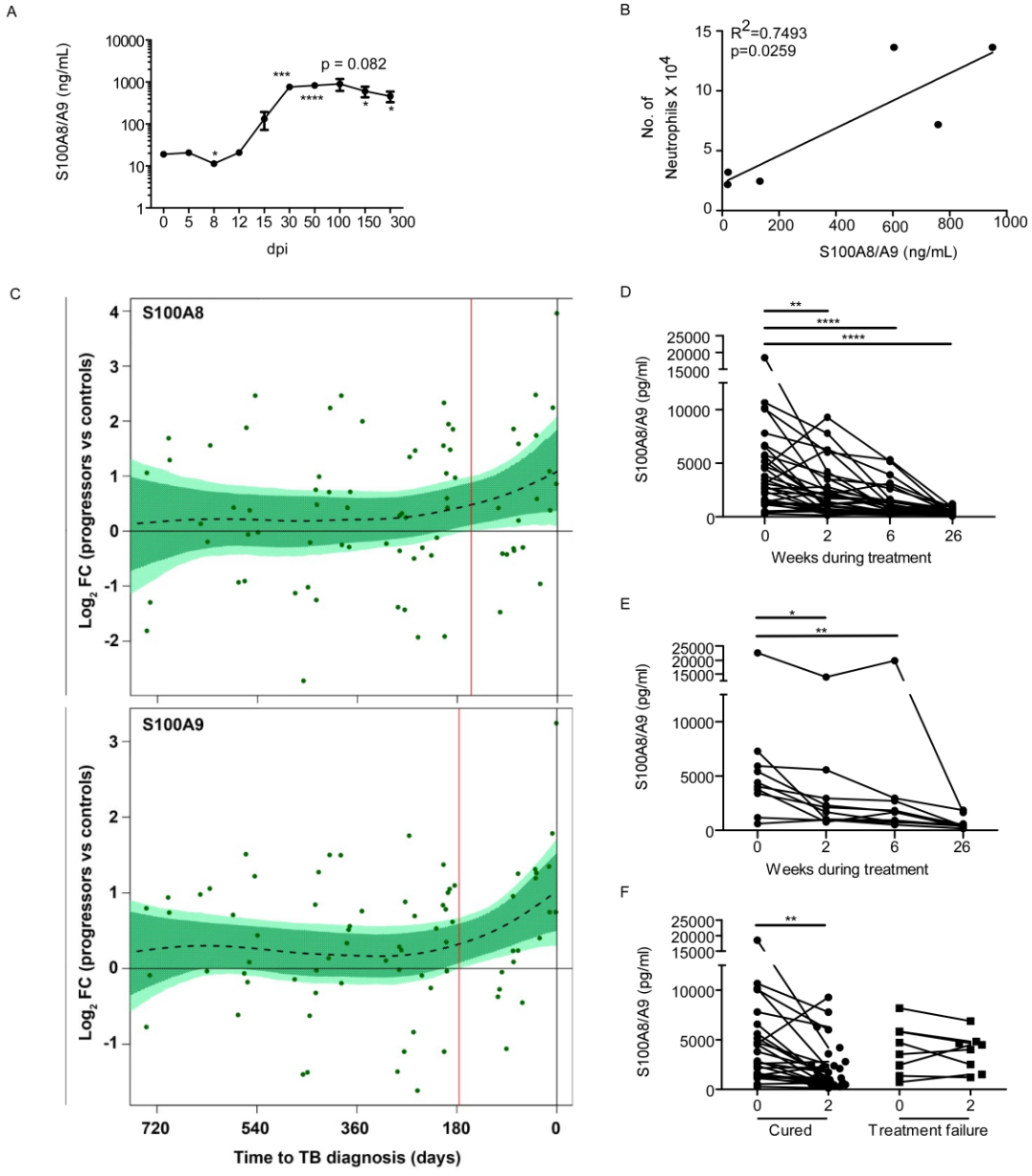

Figure 2. *S100A8/A9* mRNA levels are indicators of TB disease progression in mice and humans with TB. B6 mice (n=3-5) were aerosol-infected with ~100 CFU Mtb HN878. (A) Lung S100A8/A9 levels were determined by ELISA at dpi. (B) The number of neutrophils was correlated with the levels of S100A8/A9 using a linear regression of the means. (C) Kinetics of *S100A8* and *S100A9* mRNA expression over time, expressed as log2 fold change between bin-matched progressors (n=44) and controls (n=106) and modeled as non-linear splines (dotted lines). Light green shading represents 99% CI and dark green shading 95% CI for the temporal trends, computed by performing 2000 spline fitting iterations after bootstrap resampling from the full dataset. The deviation time (day), calculated as the time point at which the 99% CI deviates from a log2 fold change of 0, is indicated by the vertical red line. Pulmonary TB patients were enrolled and treated with standard first-line TB regimen. Serum samples were collected at time of diagnosis (0), and at weeks 2, 6 and 26 during treatment. S100A8/A9 levels were determined by ELISA in patients that were (D) successfully treated and cured (n= 34), (E) successfully treated but relapsed (n= 10), and (F) cured (n=34) vs. failed treatment (n= 10) at 2 weeks post treatment initiation. (A) Student's t-test between 0 and indicated dpi, (B) Linear regression of the means, (D-F) Mixed Effects analysis of 1-way ANOVA with Dunnett's post-test. Figures are depicting 1 experiment representative of 2, or combined data from multiple experiments. The data points represent the mean (±SEM) of values. P = 0.05 (*), P = 0.01 (**), P = 0.001 (***), and P = 0.0001 (****).

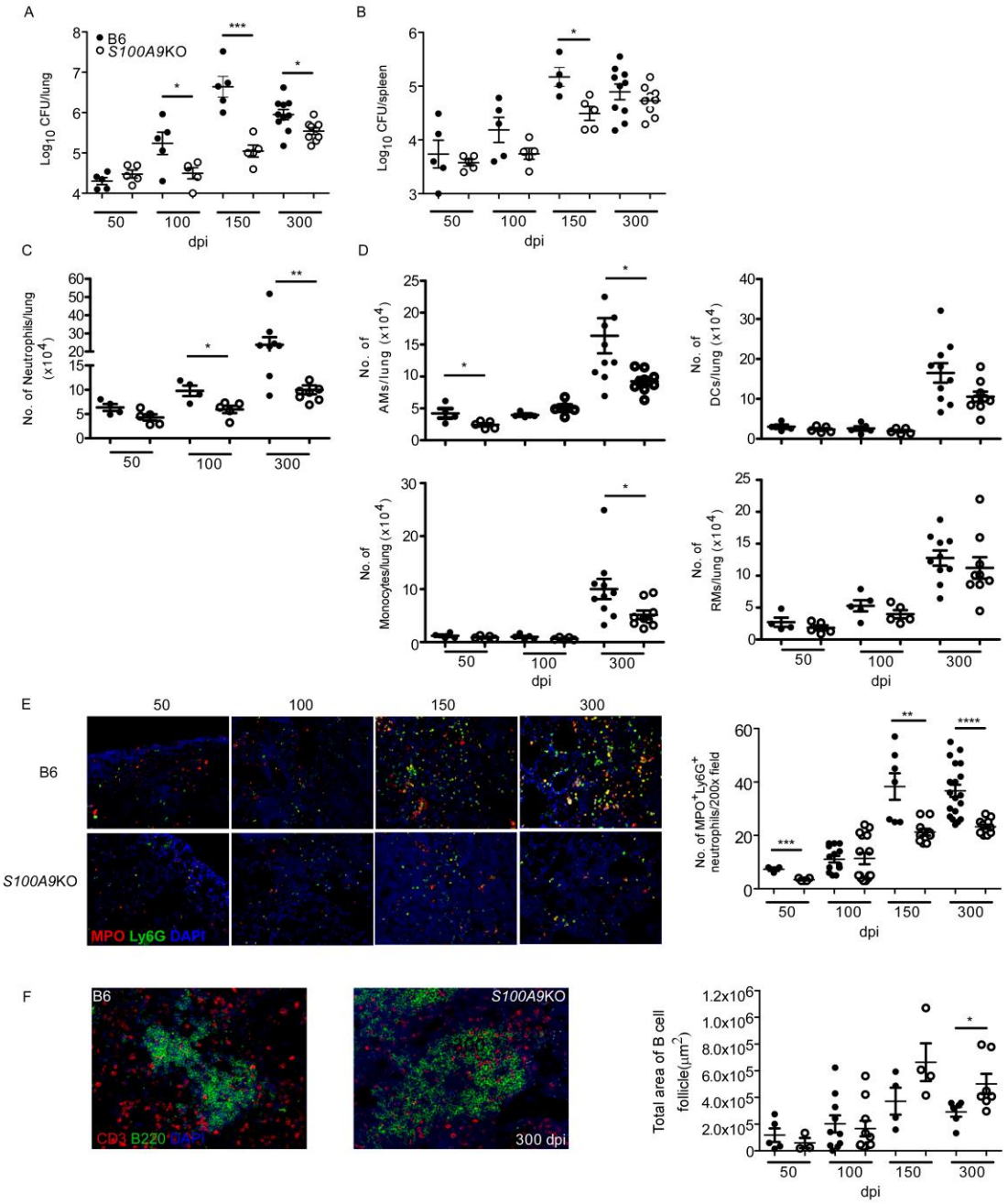

Figure 3. S100A8/A9 deficiency protects mice during chronic TB. B6 (n=5-10) and *S100A9*KO (n=5-9) mice were aerosol-infected with ~100 CFU *Mtb* HN878. (A, B) Lung and spleen bacterial burden was determined by plating at different dpi. Lung myeloid population cell counts were enumerated in B6 and *S100A9*KO HN878-infected mice using flow cytometry at 50,100,150,300 dpi and (C) neutrophils, and (D) other myeloid cells are shown. (E) FFPE lung sections were used to carry out immunofluorescence staining for Ly6G (green), MPO (red), and DAPI (blue) or B220 (green), CD3 (red) and DAPI (blue). (F) Total area occupied by B cell follicles was determined using the morphometric tool of the Zeiss Axioplan microscope at 200× magnification. AMs: alveolar macrophages, DCs: dendritic cells, RMs: recruited macrophages. Figures are depicting 1 experiment representative of 2, or combined data from multiple experiments. The data points represent the mean (±SEM) of values. (A-F) Student's t-test between B6 and *S100A9*KO at each indicated timepoint. P = 0.05 (*), P = 0.01 (**), P = 0.001 (***), and P = 0.0001 (****).

831

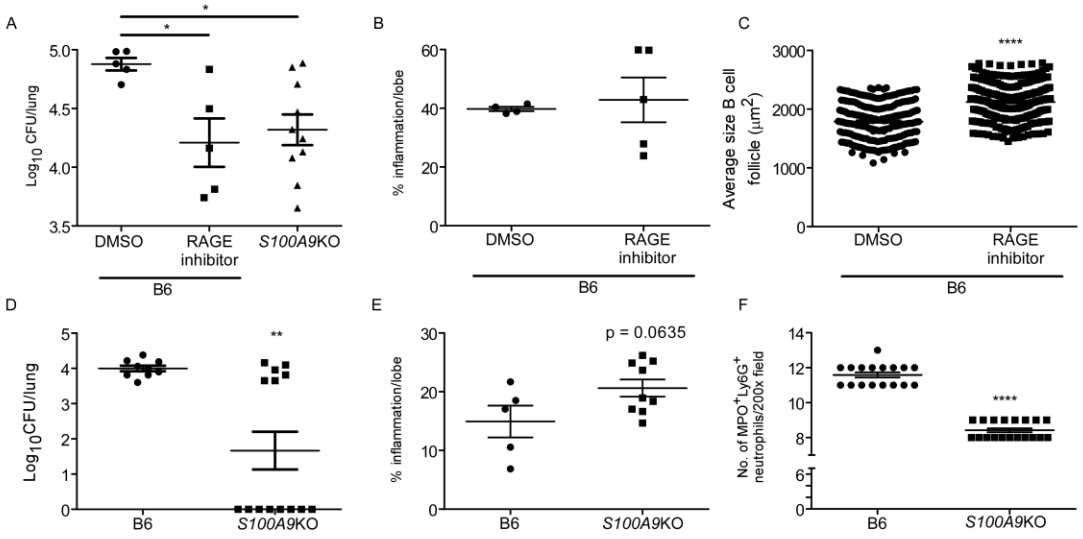

Figure 4. Targeting the S100A8/A9 pathway limits susceptibility to chronic TB and TB reactivation. *Mtb*-infected B6 and *S100A9*KO (n=10) mice were treated with RAGE inhibitor (1 mg/kg RAGE-specific blocker FPS-ZM1 (n=5) or DMSO in PBS (n=5)) at 205 dpi for 15 days and (A) lung bacterial burden at 220 dpi was determined by plating, (B) pulmonary inflammation was quantified on FFPE lung sections stained with H&E and (C) area occupied by B cell follicles was quantified histologically. B6 (n=9) or *S100A9*KO (n=13) infected mice were treated with rifabutin (100 mg/l) and isoniazid (200 mg/l) for 6 weeks and mice organs were then harvested and homogenized at 140 dpi to determine reactivation of *Mtb* infection. (D) Lung bacterial burden was determined by plating, (E) pulmonary inflammation was quantified on FFPE lung sections stained with H&E, and (F) quantification of MPO^+Ly6G^+ neutrophils was carried out in FFPE lung sections. Figures are depicting 1 experiment representative of 2, or combined data from multiple experiments. The data points represent the mean (±SEM) of values. (A) 1-way ANOVA with Tukey's post-test, (B-F) Student's t-test between groups. P = 0.05 (*), P = 0.01 (**), and P = 0.0001 (****).

832

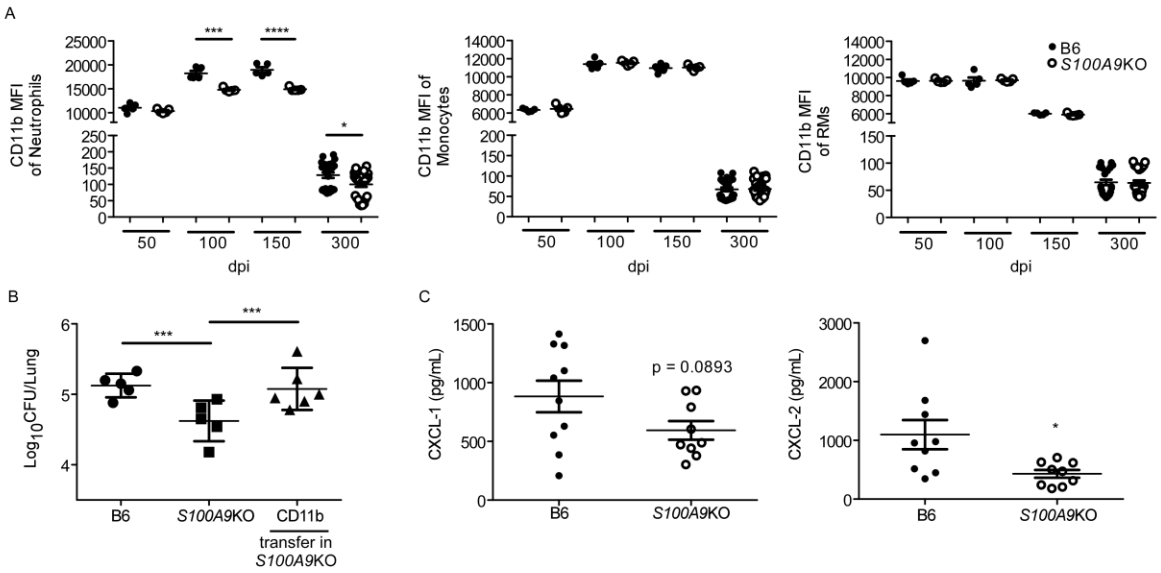

Figure 5. CD11b$^+$ cells mediate improved protection in *S100A9*KO *Mtb*-infected mice. B6 (n=5-24) and *S100A9*KO (n=5-24) mice were aerosol-infected with ~100 CFU *Mtb* HN878. (A) CD11b mean fluorescence intensity (MFI) on neutrophils, monocytes and RMs was determined using flow cytometry at 50, 100, 150 and 300 dpi. *S100A9*KO (n=6) infected mice received CD11b$^+$ purified cells from B6 mice (50 µl containing 1x10^6 cells) intratracheally at 100 dpi. (B) Lung bacterial burden was determined by plating at 120 dpi. (C) Lung homogenates were analyzed by Luminex for CXCL-1 and CXCL-2 at 300 dpi. Figures are depicting 1 experiment representative of 2, or combined data from multiple experiments. The data points represent the mean (±SEM) of values. (A, C) Student's t-test between B6 and *S100A9*KO per timepoint, (B) 1-way ANOVA with Tukey's post-test. P = 0.05 (*), P = 0.001 (***), and P = 0.0001 (****).

833

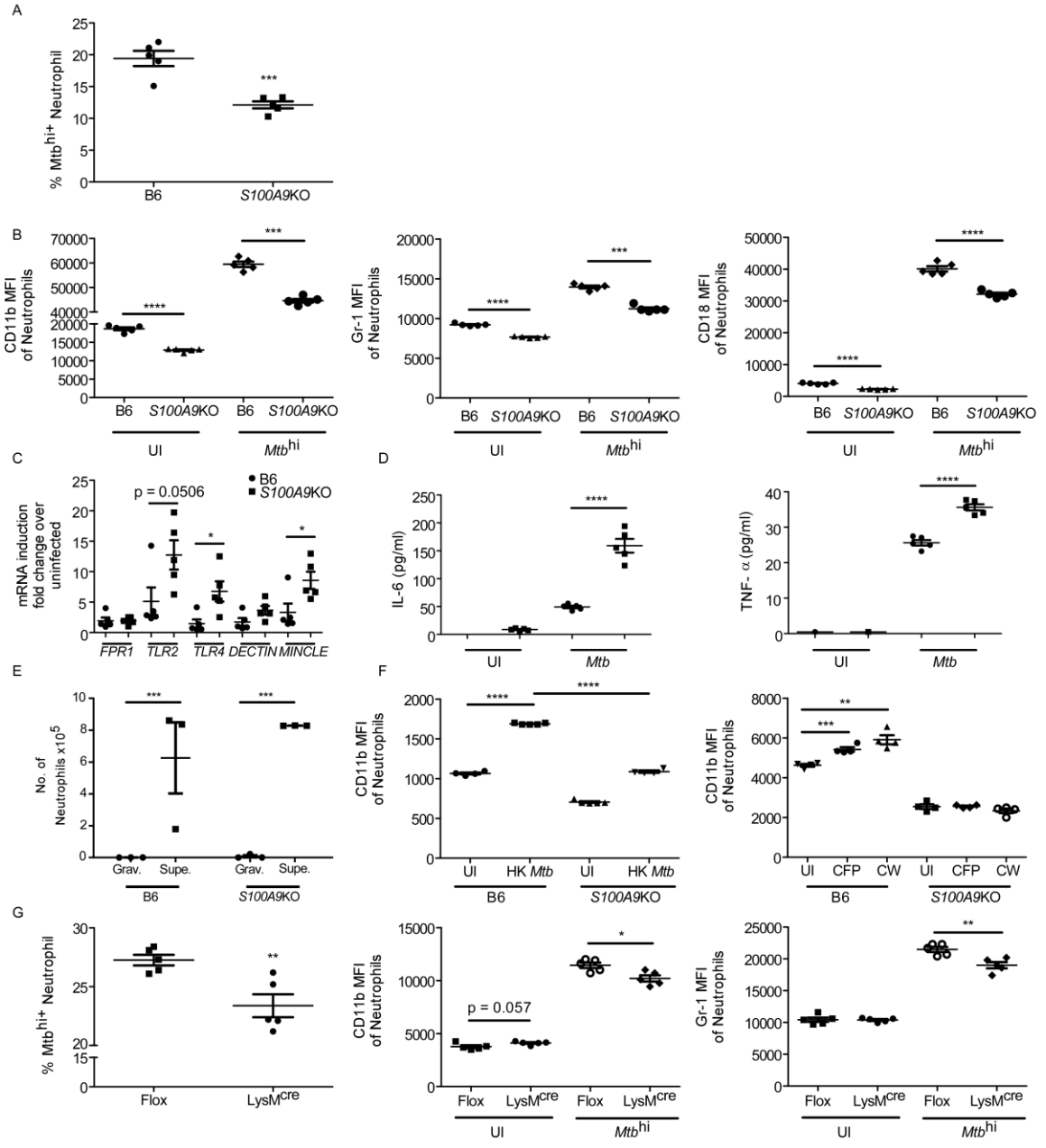

Figure 6. S100A8/A9 regulates CD11b expression on neutrophils. Bone marrow neutrophils were isolated and infected with mCherry labeled HN878 (MOI of 1) for 3 hours. (A) *Mtb* uptake by neutrophils was determined in B6 (n=5) and *S100A9*KO (n=5) neutrophils using flow cytometry. (B) MFI of CD11b, Gr-1 and CD18 expression on uninfected (UI) and highly infected (*Mtb*^{hi}) neutrophils was determined by flow cytometry. Bone marrow neutrophils were isolated and infected with HN878 (MOI of 1) for 3 hours. (C) Expression of phagocytic markers quantitated via RT-PCR, and (D) TNF-a and IL-6 levels as quantitated by Luminex assays. Bone marrow neutrophils were isolated from B6 (n=5) and *S100A9*KO (n=5) mice and infected with HN878 (MOI of 1) for 1 hour. (E) Neutrophils chemotactic activity was assayed against gravity controls (closed circles), or supernatants from infected epithelial cells (closed squares). Neutrophils from B6 mice were left untreated (UI) or treated with heat killed *Mtb* (HK), *Mtb* culture filtrate protein (CFP) and Mtb cell wall preparations (CW). (F) CD11b and Gr-1 MFI was assessed using flow cytometry. Bone marrow neutrophils from IKK$^{fl/fl}$ LysM^{Cre} mice (n=5) and IKK$^{fl/fl}$ (n=5) mice were infected with *Mtb* (MOI 1). (G) *Mtb* uptake, and MFI of CD11b and Gr-1 expression on uninfected or infected neutrophils was determined by flow cytometry. Figures are depicting 1 experiment representative of 2, or combined data from multiple experiments. The data points represent the mean (±SEM) of values. (A-G) Student's t-test. P = 0.05 (*), P = 0.01 (**), P = 0.001 (***), and P = 0.0001 (****).

834

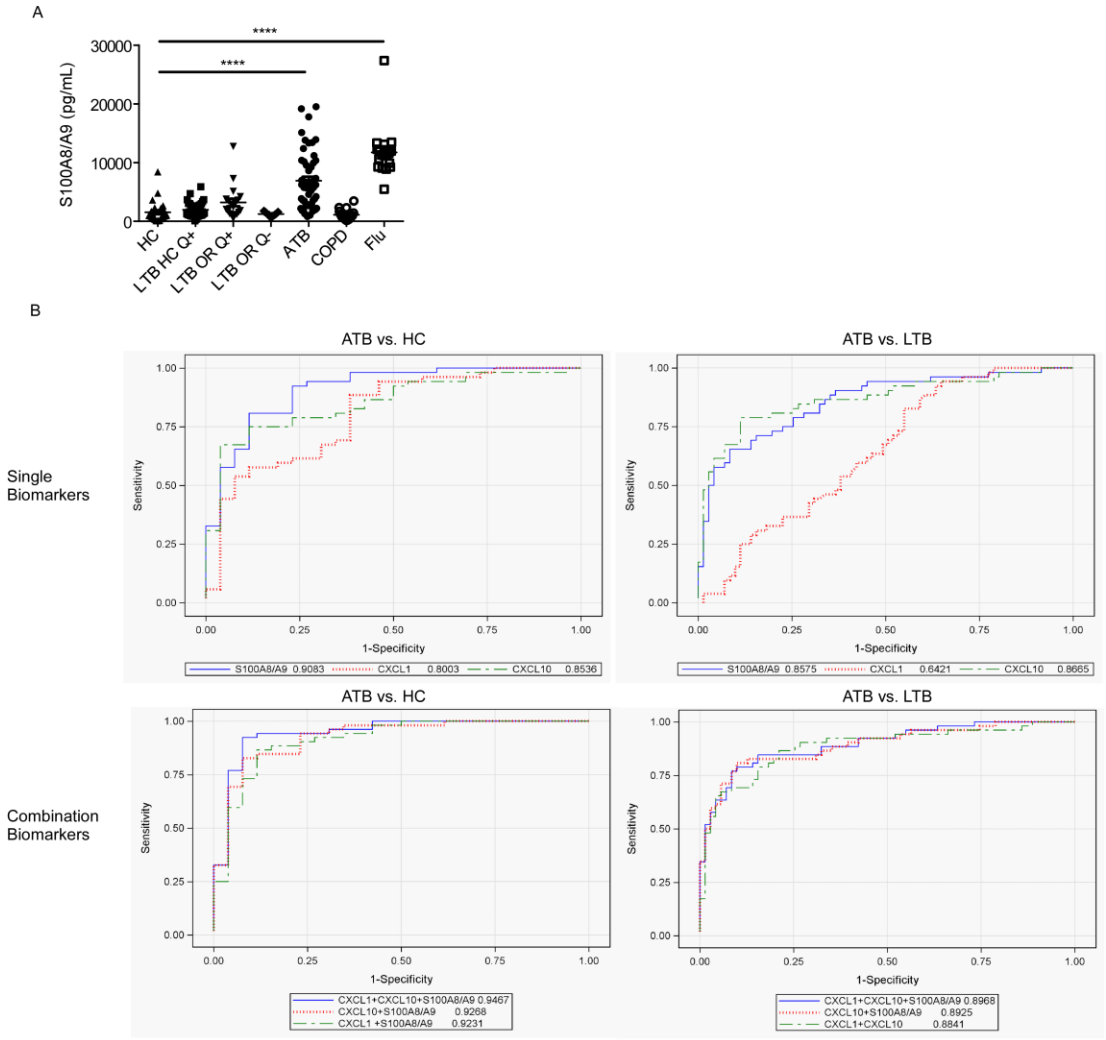

Figure 7. S100A8/A9 proteins can distinguish between ATB and healthy controls. Heathy uninfected controls (TST-QFT-) (n=26), LTBI household contacts (TST+QFT+LTBI) (n=36), LTBI occupational exposed individuals who are TST+QFT+ (n=19), LTBI occupational risk individuals who are TST+QFT- (n=9), ATB (n=52), patients with chronic obstructive pulmonary disease (COPD) (n=16), and influenza (Flu) (n=18) patient serum were collected and (A) S100A8/A9 levels were determined by ELISA. Groups were compared with a 1-way ANOVA with Dunnett's post-test. (B) ROC curves of single (top panel) and top 3 biomarker combinations (bottom panel) for ATB vs HC (left panel) and ATB vs LTBI (right panel) shown. P = 0.05 (*) and P = 0.0001 (****).

835